Appl Phys B (2008) 93: 859–864
DOI 10.1007/s00340-008-3251-8

Applied Physics B
Lasers and Optics

Optical parameters of nanostructured thin films of electromagnetite $Pb_{1-x}Sr_x(Fe_{0.012}Ti_{0.988})O_3$

K.C. Verma · P. Sharma · N.S. Negi

Received: 14 June 2008 / Revised version: 30 August 2008 / Published online: 21 October 2008

Abstract Polycrystalline $Pb_{1-x}Sr_x(Fe_{0.012}Ti_{0.988})O_3$ ($0.2 \leq x \leq 0.4$) (PSFT) thin films have been grown on fused quartz substrates by metallo-organic decomposition technique. The grown films were characterized using X-ray diffraction (XRD), atomic force microscopy (AFM), source meter and UV–Vis–NIR spectrophotometer to determine the structural, microstructural, dc resistivity and optical properties. The XRD pattern confirmed that the PSFT films has distorted tetragonal single phase, which close to cubic at higher Sr concentration. AFM analysis revealed that the grains size reduces with increasing Sr concentration and their average values lies in the range of 26–9 nm. The higher values of dc resistivity of PSFT nano grains indicate that the transmission of light occurs within these grains up to short wavelength. The refractive index and the extinction coefficient were determined from the optical transmission spectrum in the wavelength range of 200–1100 nm and compared with that theoretically calculated, when fitted to a single oscillator model. The values of optical band gap were determined from Tauc's extrapolation fitting and suggests that the transformation of electrons during transmission of light through local states within Fermi gap.

PACS 73.63.Bd · 72.30.+q · 78.20.-e · 78.66.-w · 78.67.-n

K.C. Verma (✉) · N.S. Negi
Department of Physics, Himachal Pradesh University, Shimla 171005, India
e-mail: kuldeep0309@yahoo.co.in

P. Sharma
Department of Physics, Jaypee University of Information Technology, Waknaghat, Solan 173215, India

1 Introduction

At present there is an active search for materials displaying the coexistence of ferromagnetism and ferroelectricity, so-called magnetoelectric materials. Among them, the perovskite compounds of $PbTiO_3$ exhibit a remarkable magnetoelectric effect, when doped with transition metal ions, i.e. Fe, Co, Ni, etc., for growing it either in thin film form or as nanoparticles [1–3]. However, the electromagnetite compounds of $Pb(FeTi)O_3$ (PFT) become appreciable for optical components when the light transmit through their nano sized grains. The doping of Sr into A-site of PFT compound can reduce the grains size into the smallest possible limit [4] and makes it suitable for various surface plasmon (SP) made devices [5–8]. When the wavelength of incident electromagnetic field coincided with the resonance wavelength of metal nanoparticles, the surface plasmon would be excited. The resonant interaction between the surface charge oscillation and the electromagnetic field of the light constitutes the SP and gives rise to its unique properties. The SP have potential in optics such as magneto-optic data storage, microscopy and solar cells, as well as being used to construct sensors for detecting biologically interesting molecules. In despite of surface plasmon, the small grains create large insulating boundaries between them, which required higher frequency of light when transmitting it through these grains boundaries. Therefore, transmission of light within nano grains offers large electro-optic coefficient [9], large absorbance and transmittance of light in its short wavelength region and attributes large value of refractive index to make dense optical signal in various optical fiber-based systems. Bhardwaj et al. [10] prepared $Pb_{1-x}Fe_xSe$ nanoparticles thin film and demonstrated structural, optical and electrical parameters. There was found some inconsistency to the confirmation of crystalline phase, grains size and optical

constants and observed small value of resistivity of nanoparticles (in the order of 10^4 Ω cm). In our previous system of PFT nanoparticles [3], the calculated value of resistivity was in the order of 10^{10} Ω cm, which makes it suitable for higher frequency applications. The effect of Sr substitution into multiferroic PFT system to make reducible small, uniformly compact and closed packed nanoparticles and the resulting magnetic and electric properties to be improved were also studied [11]. The present system of nanostructured $Pb_{1-x}Sr_x(Fe_{0.012}Ti_{0.988})O_3$ demonstrating the dc resistivity in the order of 10^{11} Ω cm at room temperature, which makes these nano-grains suitable for those optical components which require higher energy for device manufacturing.

In this paper we report the preparation and characterisation of $Pb_{1-x}Sr_x(Fe_{0.012}Ti_{0.988})O_3$ (PSFT) ($0.2 \leq x \leq 0.4$) nanocrystalline thin films prepared by metallo-organic decomposition (MOD) technique. The different optical parameters such as refractive index (n), extinction coefficient (k) and absorption coefficient (α) are calculated from the transmission spectrum by Swanepoel method [12]. The optical band gap, optical dielectric constant are also calculated by Tauc's extrapolation method [13].

2 Experimental

PSFT thin films were prepared using lead 2-ethylhexanoate $(C_7H_{15}COO)_2Pb$ with 20 mol% Pb in excess, strontium 2-ethylhexanoate $(C_7H_{15}COO)_2Sr$, iron 2-ethylhexanoate $(C_7H_{15}COO)_2Fe$ and tetra-n-butyl orthotitanate as precursor solutions. The coating solution was prepared by mixing the precursor solutions in the desired molar ratio of Pb:Sr:Fe:Ti. Under the influence of constant stirring, the solution was refluxed at 120°C for 10 h for homogeneous mixing. By using spin coating technique, the solution was coated on fused quartz substrates with spinning speed of 4300 rpm for 60 s. After spinning onto the substrates, the films were subjected at 350°C for 5 minutes to remove the solvent and organic residuals. In order to improve film thickness, the coating and baking steps were sequentially repeated for three times. A post-deposition isothermal annealing of spin-on coating at 650°C for all samples in an oxygen atmosphere for 3 h leads to crystalline PSFT films. The thickness of the films is measured by using the Talystep stylus instrument (Embios Technology). The final thickness of PSFT film after three coating is ∼400 nm. The phase structure and grain's size of the film is analysed by X-ray diffraction (XRD) using X-pert PRO and morphology by atomic force microscopy (AFM) using VECCO DI CP-II. The optical transmittance of PSFT is measured using Perkin Elmer Lambda-750 spectrophotometer in the wavelength range of 200–1100 nm. The dc resistivity of PSFT thin films was measured using Keithley 2611 source meter.

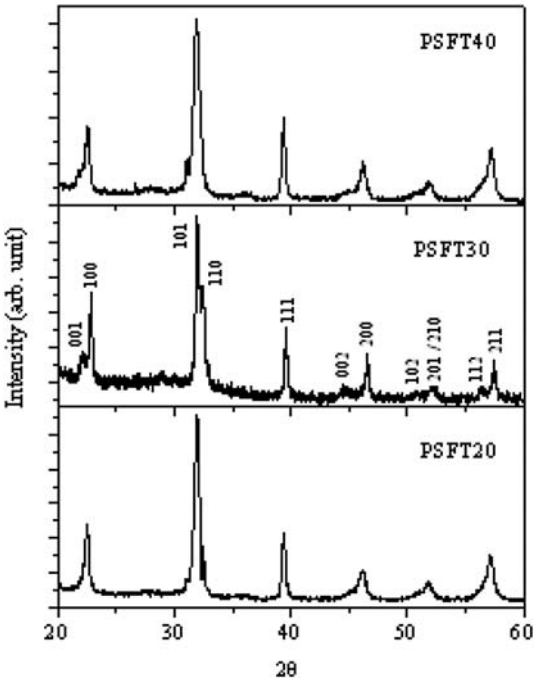

Fig. 1 XRD of PSFT thin films grown with 20% of Sr (PSFT20), 30% of Sr (PSFT30) and 40% of Sr (PSFT40) concentrations

3 Results and discussions

Figure 1 shows the XRD patterns of PSFT thin films grown with 20% Sr (PSFT20), 30% Sr (PSFT30) and 40% Sr (PSFT40) concentrations. All the films were deposited on fused quartz substrates and annealed at 650°C of temperature. The XRD peaks in PSFT films can be identified to come from the distorted tetragonal phase, and the absence of any pyrochlore phase except PSFT40 confirmed their polycrystalline nature. The impurity phase of PSFT40 film exists because of higher Sr concentration reported in the literature [14]. The distortion (c/a) is significantly decreased when increasing Sr-doping and lies in the range of 1.0036–1.0011. These values of c/a are very small as compared with parent $PbTiO_3$(1.066) compound. This result confirms that the distorted tetragonal PSFT phase is very close to cubic when the Sr concentration is high. Hence, the resulting formation of PSFT grains is uniformly compact and closely packed, and within it the transmission of light is improved. Assuming the broadening to come primarily from grains size, we used the Scherrer formula [15] to find the average grain size. Table 1 gives the values of lattice distortion and average grain size. The calculated values of grain size lie in the range of nm for all PSFT films. The reduction of grain size with increasing Sr concentration may be attributed to the lower grain-growth rates due to the slower diffusion of Sr^{2+} ion. Crystallisation may be initiated earlier with lower Sr content, resulting into a larger grain size for the same heat treatment [16].

The AFM images of PSFT thin films grown with different Sr concentrations are shown in Figs. 2(a) to 2(c). The

Table 1 Values of grain size (x), optical film thickness (d), distortion ratio (c/a), single oscillator energy (E_o), dispersion energy (E_d), static refractive index (n_o), optical energy band gap (E_g^{opt}) and dc resistivity for PSFT thin films

Composition	x (nm)	d (nm)	c/a	E_o (eV)	E_d (eV)	n_o	E_g^{opt} (eV)	ρ (10^{11} Ω cm)
PSFT20	26	289	1.0036	3.66 ± 0.02	7.01 ± 0.5	1.71	1.833 ± 0.01	3.3
PSFT30	17	386	1.0027	3.81	10.33 ± 0.4	1.93	1.904	1.01
PSFT40	9	509	1.0011	3.59 ± 0.01	5.564	1.59	1.797 ± 0.02	0.42

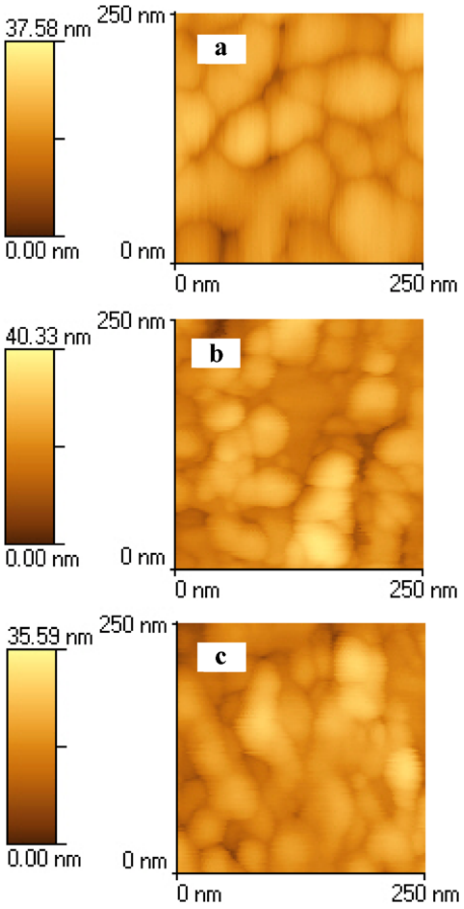

Fig. 2 AFM of PSFT thin films grown with (**a**) 20% Sr, (**b**) 30% Sr and (**c**) 40% Sr concentrations

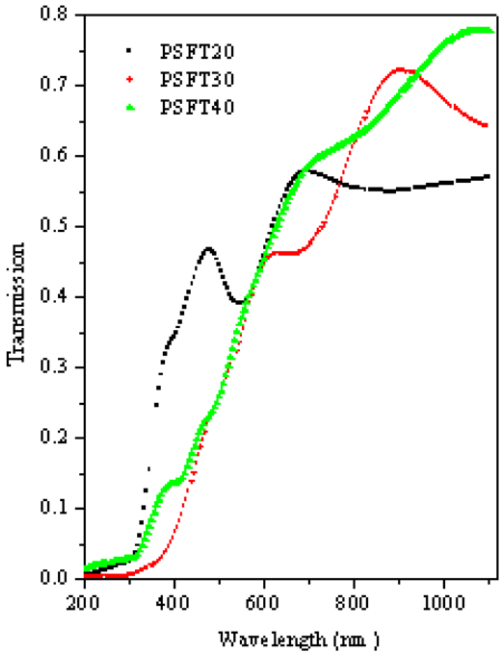

Fig. 3 Transmission versus wavelength for PSFT thin films

AFM indicates that the PSFT films are smooth; crack free, small surface roughness and grains in nano-size (Table 1). The AFM images of PSFT film showed the roughness values 3 nm, 2.1 nm and 2.2 nm and the average grain size values 25 nm, 15 nm and 10 nm, respectively. These observed values of grain size from AFM are consistent with that calculated from XRD peaks using Scherer's relation. These nano-sized grains contain large insulating boundaries between them and create a barrier for conduction of electrons from valence band to conduction band. Hence, this results in the increase of resistivity, and the transformation of electrons takes place through local states within the Fermi gap. The observed value of dc resistivity at room temperature for PSFT nano-grains with different Sr concentrations is in the order of 10^{11} Ω cm and given in Table 1. A small reduction in the values of resistivity is observed when increasing Sr content, indicating the formation of uniform grains, which are arranged as in close-packed, ordered nano-grains super lattices.

Optical properties of PSFT thin films grown with different Sr concentrations were determined from the optical transmission spectra recorded in the wavelength range of 200–1100 nm. The transmission of light through PSFT films when deposited on fused quartz substrates and annealed at 650°C is shown in Fig. 3. The transmission curve indicated the absence of any abrupt decrease of transmittance up to short wavelength region of light. The film grown at higher Sr concentration (40% Sr) explained slightly large transmittance than that grown at lower Sr content (20% Sr, 30% Sr). The large transparency in the films confirmed the presence of small, uniform and closely packed grains. It is also found that at even small wavelength ~400 nm (short wavelength

region), the absorption and transmission of light takes place that makes PSFT nano-grains possible for the surface plasmon (SP) devices [6] existing on the metal surface. The use of SPs to help us concentrate light in subwavelength structures stems from the different (relative) permittivities, ε, of the metals and the surrounding non-conducting media [17]. The surface plasmon polaritons (SSP) are Bragg reflectors built from periodically arranged lines of nanoscale metal protrusions or indentations on a metal film [18]. This opens a possibility for spectral demultiplexing if we put different Bragg mirrors in series such that for each mirror is satisfied at different SPP wavelengths.

According to Swanepoel [12], the value of refractive index of the film can be calculated by using the following expression. In the weak region where the absorption coefficient $\alpha \neq 0$, the refractive index (n) is given by

$$n = \left[N + \left(N^2 - S^2\right)^{1/2}\right]^{1/2}, \tag{1}$$

$$N = 2S\frac{T_M - T_m}{T_M T_m} + \frac{(S^2+1)}{2}, \tag{2}$$

where T_M and T_m are the transmission values corresponding to the tangent points between the upper and lower envelops, respectively. The film thickness, d, was obtained using the relationship

$$d = \frac{\lambda_1\lambda_2}{2(\lambda_1 n_2 - \lambda_2 n_1)}, \tag{3}$$

where n_1 and n_2 are the refractive indices of two adjacent maxima or minima at wavelengths λ_1 and λ_2, respectively. The calculated values of d for PSFT thin films are given in Table 1.

The extinction coefficient (k) is calculated using the relation

$$k = \frac{\alpha\lambda}{4\pi}, \tag{4}$$

where α is the absorption coefficient and is given by

$$\alpha = \left(\frac{1}{d}\right)\ln\left(\frac{1}{x}\right), \tag{5}$$

where x is the absorbance.

The variation of refractive index (n) and extinction coefficient (k) with wavelength for nanostructured PSFT thin film grown with different Sr content is shown in Fig. 4. All calculated values of refractive index (n) are stable up to a higher frequency region ($\lambda \sim 400$ nm) of light. The films under study show large values of n, especially observed in the short wavelength region of light, which are not found in the similar literature on optical thin films of chalcogenide semiconducting glasses or mixed metal glass system [19, 20]. These nanostructured films absorb large light

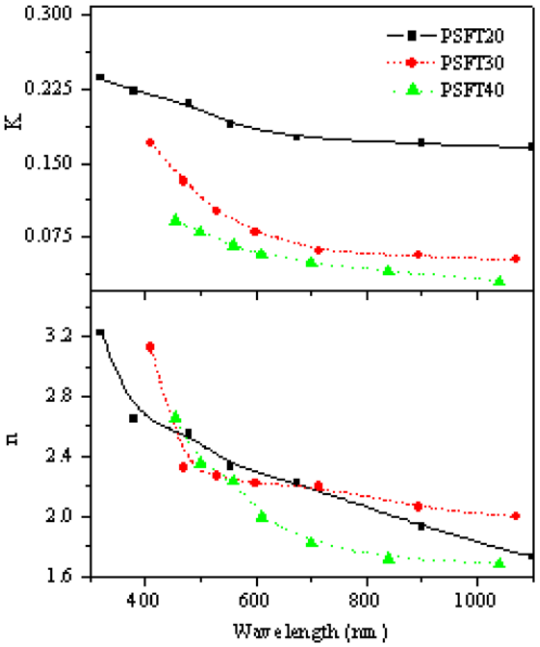

Fig. 4 Variation of refractive index (n) and extinction coefficient (k) with wavelength

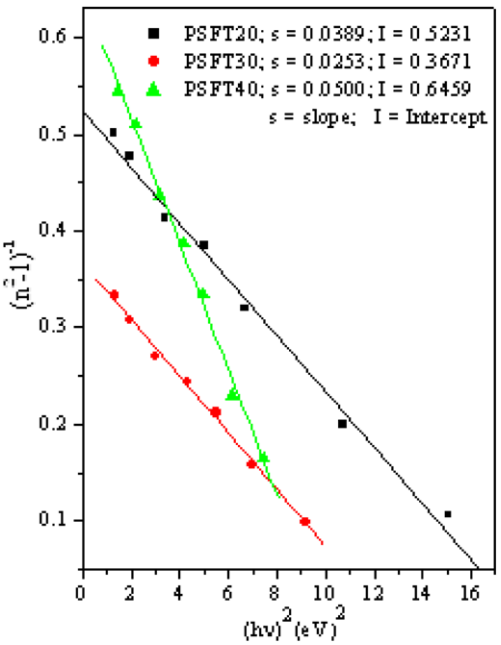

Fig. 5 Plot of refractive index factor $(n^2-1)^{-1}$ versus $(h\nu)^2$

and make highly confined wave-guides that result into dense optical signals for optical fiber based devices. The calculated values of extinction coefficient (k) indicate low lost of light during scattering and absorption. According to the

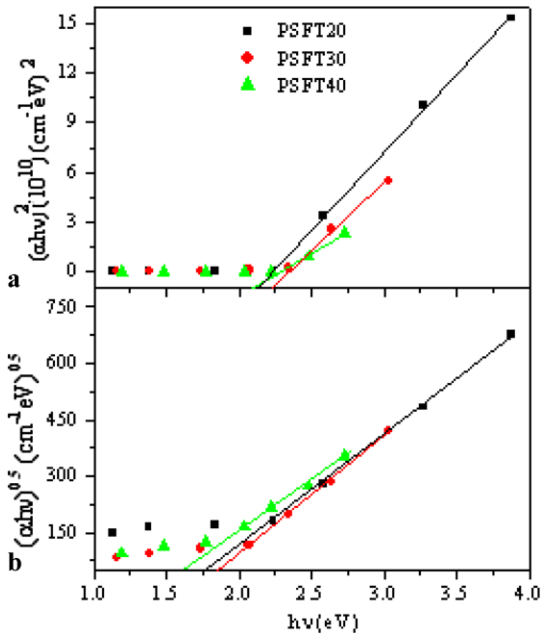

Fig. 6 (**a**) $(\alpha h\nu)^2$ versus photon energy $(h\nu)$ and (**b**) $(\alpha h\nu)^{1/2}$ versus photon energy $(h\nu)$

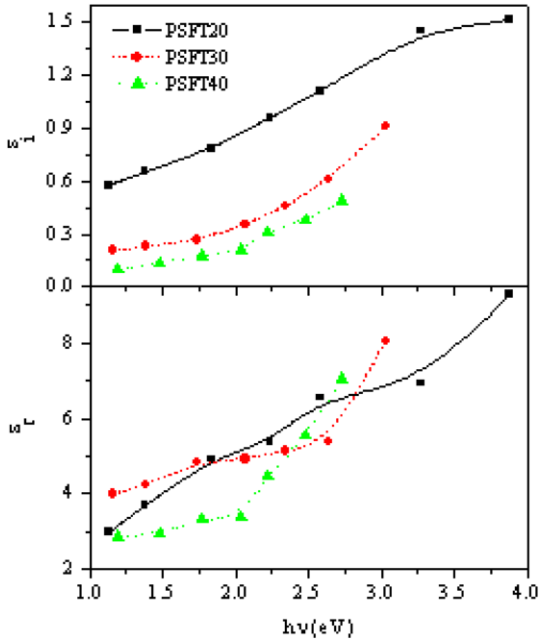

Fig. 7 Variation of optical dielectric constant (ε_r) and loss factor (ε_i) with photon energy $(h\nu)$

single-electronic-oscillator model proposed by DiDomenico and Wemple [21],

$$n^2 - 1 = \frac{E_d E_o}{E_o^2 - (h\nu)^2}, \tag{6}$$

where $h\nu$ is the photon energy, n is the refractive index, E_o is the single oscillator energy, also called average energy gap, and E_d is the dispersion energy, which is a measure of the average strength of the interband optical transitions. To analyse the above formula for PSFT films, we have linearly fitted the quantity $(n^2 - 1)^{-1}$ versus $(h\nu)^2$ for PSFT films (Fig. 5). The values of E_o and E_d are directly determined from the slope, $(E_o E_d)^{-1}$, and the intercept, E_o/E_d. It is the experimental variation in the refractive index instead of absorbance, which departs from that given by (6) when the photon energy approaches the optical band-gap [22]. The values of the dispersion parameters E_o and E_d, the corresponding static refractive index n_o (at $h\nu \to 0$) and optical band gap E_g^{opt} ($E_o \approx 2 \times E_g^{\text{opt}}$) for PSFT films are listed in Table 1. Furthermore, E_d also obeys the simple empirical relationship [21]

$$E_d = \beta N_c Z_a N_e \text{ (eV)}, \tag{7}$$

where N_c is the coordination number of the cation nearest-neighbour to the anion, Z_a is the chemical valency of the anion, and N_e is the effective number of valence electrons per anion. The values of β for ionic and covalent compounds are 0.26 ± 0.03 eV and 0.37 ± 0.04 eV, respectively. The calculated values of E_d for PSFT films using (6) are in good agreement with that from (7).

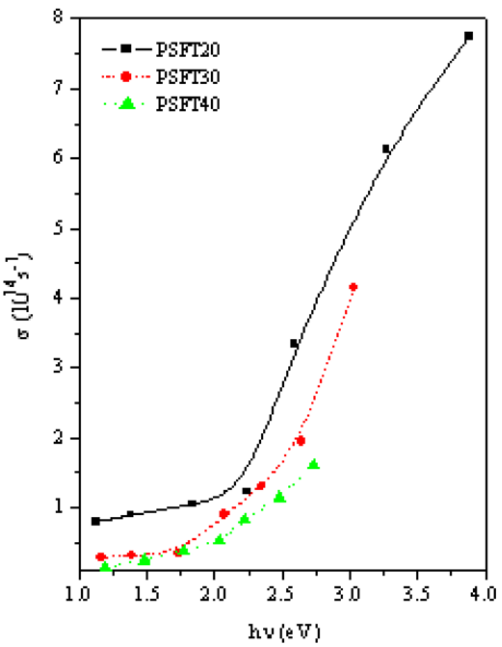

Fig. 8 Optical conductivity (σ) versus photon energy $(h\nu)$

The band gap E_g of the PSFT films cannot be obtained accurately by extrapolating the linear portion of the plot of $(\alpha h\nu)^2$ against photon energy to $(\alpha h\nu)^2 = 0$ (Fig. 6(a)). This value of the band gap is lower than those of the band gaps of parent $PbTiO_3$ (i.e. 3.7 eV) and $SrTiO_3$ (i.e. 3.2 eV). In fact, the PSFT nano-grains have large resistivity (in the order of 10^{11} Ω cm), which explained in the last section, and hence the electrons transport takes place through defect

states within Fermi gap. A satisfactory result for band gap is obtained by fitting the band gap in the plot of $(\alpha h\nu)^{1/2}$ versus $h\nu$ using Tauc's relation [13]

$$\alpha h\nu = A\left(h\nu - E_g^{\text{opt}}\right)^{1/2}, \tag{8}$$

where A is a constant, and the other symbols have their usual meaning. The values of energy band gap given by (8) are in good agreement with those calculated by Wemple–DiDomenico relation in Table 1. The real and imaginary parts of optical dielectric constant are shown in Fig. 7 by the relations [23]

$$\varepsilon_r = n^2 - k^2 \tag{9}$$

and

$$\varepsilon_i = 2nk. \tag{10}$$

The real part of the dielectric constant indicates the speed of light when it is transmitting through nano grains, and the imaginary part shows how a dielectric absorbs energy from an electric field due to dipole motion. The values of dielectric constant are 6.9, 5.9 and 7.1, respectively, observed at higher energy of 3.1 eV when the PSFT films are grown at 20, 30 and 40% of Sr concentrations.

The optical conductivity means how the dielectric can absorb light during scattering process—this observation of light is given by plotting the optical conductivity versus photon energy (Fig. 8) for PSFT films—and is given by the relation [24]

$$\sigma = \frac{\alpha nc}{4\pi}, \tag{11}$$

where c is the velocity of light, α is the absorption coefficient and n is the refractive index. The optical conductivity is found to increase sharply after 2.3 eV. At this energy region, the observed values of optical conductivity are in the order of 10^{14} s^{-1}.

4 Conclusions

The effect of Sr concentration in PSFT thin films to reduce the grains size has been observed. The PSFT solution was prepared by chemical synthesis (i.e. metallo-organic decomposition) and deposited on fused quartz substrates using spin-coating technique. The XRD and AFM show that the PSFT films are polycrystalline, and the calculated values of average grain size lie in the range ~26–9 nm. The higher value of dc resistivity is observed, which makes PSFT nano grains suitable to absorb and transmit more light up to short wavelength region and applicable for various surface plasmon devices. The optical band gaps of PSFT films are in good agreement with Wemple–DiDomenico single oscillator model and suggest that the movement of electrons takes place through defect states within the Fermi gap.

References

1. V.R. Palkar, S.C. Purandare, S. Gohil, J. John, S. Bhattacharya, Appl. Phys. Lett. **90**, 172901 (2007)
2. Z. Ren, G. Xu, X. Wei, Y. Liu, X. Hou, P. Du, W. Weng, G. Shen, G. Han, Appl. Phys. Lett. **91**, 063106 (2007)
3. K.C. Verma, R.K. Kotnala, N.S. Negi, Appl. Phys. Lett. **92**, 152902 (2008)
4. F.M. Pontes, S.H. Leal, M.R.M.C. Santos, E.R. Leite, E. Longo, L.E.B. Soledade, A.J. Chiquito, M.A.C. Machado, J.A. Varela, Appl. Phys. A **80**, 875 (2005)
5. G. Laurent, N. Felidj, S.L. Truong, J. Aubard, G. Levi, J.R. Krenn, A. Hohenau, A. Leitner, F.R. Aussenegg, Nano Lett. **5**(2), 253 (2005)
6. D. Zhang, P. Wang, J. Zhou, Y. Sun, X. Jiao, Y. Deng, H. Ming, Q. Zhang, Z. Zhang, Appl. Phys. B **84**, 239 (2006)
7. A. Drezet, D. Koller, A. Hohenau, A. Leitner, F.R. Aussenegg, J.R. Krenn, Nano Lett. **7**(6), 1697 (2007)
8. A. Christ, O.J.F. Martin, Y. Ekinci, N.A. Gippius, S.G. Tikhodeev, Nano Lett. **8**, 2171 (2008)
9. M. Gaidi, M. Chaker, P.F. Ndione, R. Morandotti, B. Bessais, J. Appl. Phys. **101**, 063107 (2007)
10. A. Bhardwaj, E. Varadarajan, P. Srivastava, H.K. Sehgal, Solid State Commun. **146**, 53 (2008)
11. K.C. Verma, M. Singh, R.K. Kotnala, N.S. Negi, Appl. Phys. Lett. **93**, 072904 (2008)
12. R. Swanepoel, J. Phys. E **16**, 1214 (1983)
13. J. Tauc, A. Menth, J. Non-Cryst. Solids **8**, 569 (1972)
14. R. Thomas, D.C. Dube, M.N. Kamalasanan, S. Chandra, A.S. Bhalla, J. Appl. Phys. **82**, 4484 (1997)
15. B.D. Cullity, *X-ray Diffraction* (Addison-Wesley, Reading, 1967)
16. M.C. Gust, L.A. Momoda, N.D. Evans, M.L. Mecartney, J. Am. Ceram. Soc. **84**, 1087 (2001)
17. W.L. Barnes, A. Dereux, T.W. Ebbesen, Nature **424**, 424 (2003)
18. J.C. Weeber, M.U. Gonzalez, A.L. Baudrion, A. Dereux, Appl. Phys. Lett. **87**, 221101 (2005)
19. E. Cetinorgu, S. Goldsmith, R.L. Boxman, J. Phys. D: Appl. Phys. **39**, 1878 (2006)
20. Y.P.V. Subbaiah, P. Prathap, K.T.R. Reddy, D. Mangalaraj, K. Kim, J. Yi, J. Phys. D: Appl. Phys. **40**, 3683 (2007)
21. S.H. Wemple, Phys. Rev. B **7**, 3767 (1973)
22. I. Solomon, M.P. Schmidt, C. Senemaud, M.K. Driss, Phys. Rev. B **38**, 13263 (1988)
23. Q. Ren, Y.T. Chow, F.Q. Meng, S.W. Wang, Z.H. Lu, C.B. Ma, H. Wang, D. Xu, W.A. Gambling, J. Mater. Sci. **36**, 1857 (2001)
24. J.I. Pankov, *Optical Processes in Semiconductors* (Dover, New York, 1975), p. 91